RESEARCH ARTICLE | MAY 02 2025

Efficient treatment of long-range electrostatics in charge equilibration approaches

Kamila Savvidi ; Ludwig Ahrens-Iwers ; Lucio Colombi Ciacchi ; Dirk Zahn ; Martin H. Müser ; Robert Horst Meißner

J. Chem. Phys. 162, 174108 (2025)
https://doi.org/10.1063/5.0255823

The Journal of Chemical Physics ARTICLE pubs.aip.org/aip/jcp

Efficient treatment of long-range electrostatics in charge equilibration approaches

Cite as: J. Chem. Phys. 162, 174108 (2025); doi: 10.1063/5.0255823
Submitted: 31 December 2024 • Accepted: 10 April 2025 •
Published Online: 2 May 2025

Kamila Savvidi,[1] Ludwig Ahrens-Iwers,[1] Lucio Colombi Ciacchi,[2] Dirk Zahn,[3] Martin H. Müser,[4] and Robert Horst Meißner[1,5,a)]

AFFILIATIONS

[1] Institute for Interface Physics and Engineering, Hamburg University of Technology, Hamburg, Germany
[2] Faculty of Production Engineering, Bremen Center for Computational Materials Science, Hybrid Materials Interfaces Group and MAPEX Center for Materials and Processes, University of Bremen, Bremen, Germany
[3] Computer-Chemie-Centrum and Chair of Theoretical Chemistry Erlangen, Friedrich-Alexander-Universität Erlangen-Nürnberg (FAU), Erlangen, Germany
[4] Department of Materials Science and Engineering, Saarland University, Saarbrücken, Germany
[5] Institute of Surface Science, Helmholtz-Zentrum Hereon, Geesthacht, Germany

[a)] **Author to whom correspondence should be addressed:** robert.meissner@tuhh.de

ABSTRACT

A charge equilibration method based on real-space Gaussians as charge densities is presented. The implementation is part of the Electrode package available in the Large-scale Atomic/Molecular Massively Parallel Simulator and benefits from its efficient particle-mesh Ewald approach. A simple strategy required to switch from the previously used Slater-type orbital (STO) shielding to Gaussians is provided by fitting the Coulomb energy of two Gaussian charge distributions to the repulsion between two STOs. Their widths were optimized for O, Si, and Ti species, obtaining results consistent with previous studies using STOs in the case of SiO_2 polymorphs. In the limit of sufficiently narrow Gaussians, it is shown that the implementation converges to electronegativity equalization method results for the case of Ti/TiO_x interfaces. The method presented is implemented in a way that is potentially beneficial for the application of modern machine-learning force fields that include long-range electrostatic interactions.

INTRODUCTION

Molecular simulations[1,2] based on empirical potentials[3,4] are frequently used whenever the system sizes and time scales required to gain useful information on collective phenomena surpass those that can be tackled at the quantum mechanical level, e.g., with density functional theory (DFT) methods.[5,6] Although machine-learned potentials (MLPs)[7,8] often reduce the computational burden of DFT, they generally still require substantially more computing time than common empirical potentials. Moreover, they become more complex when (non-local) charge-transfer or polarization effects are important.[9] For example, to simulate batteries[10,11] or supercapacitors,[12,13] charge transfer at solid–liquid interfaces is of crucial importance. These are generic examples of situations in which interactions are non-local and/or where the concept of mirror charges cannot be applied in a straightforward fashion. This is due to complex interface geometries and the dynamic effects of the molecular species at the polarized electrodes. In the latter case, induced charges must be properly assigned to atoms near the metal surface to correctly reproduce the polarization-induced repulsion between near-surface atoms.

One possibility of modeling not only charge transfer but also the dielectric response of condensed matter is the use of charge-transfer potentials (CTPs), which allow partial charges of atoms to be determined on the fly. Mortier and co-authors[14,15] pioneered the most widely used CTPs by defining a potential energy function containing a second-order polynomial of the partial charge q_i, which gets minimized with respect to all q_i for a given configuration. The polynomial consists of a linear coupling to an atom, reflecting the atomic electronegativity, a quadratic self-interaction,

penalizing charge accumulation on a given atom and reflecting its chemical hardness, and a Coulomb interaction between all charges. This method, which can be loosely interpreted as an attempt to coarse-grain an electronic structure calculation to atoms, was originally introduced as the electrostatic equalization method (EEM). It has experienced various modifications, not only in terms of different approximations to the Coulomb interactions[16,17] but also with respect to its generic functional form.[18–23]

The supposedly first modifications of EEM were proposed by Rappe and Goddard,[16] who replaced the bare Coulomb potential with a shielded one by introducing radially symmetric ns-STOs of the form $\phi(r) = N_n r^{n-1}\exp(-\zeta r)$, with the normalization constant N_n, the principal quantum number n, and the orbital exponent ζ. This was done to improve the stability and accuracy of CTPs, of which both can be compromised when two atoms approach each other closely, particularly when they carry opposite charges. Rappé and Goddard called their approach charge equilibration (QEq), which has become the most commonly used term for CTPs, in which partial charges are determined by a minimization principle. We refer to three recent articles[4,24,25] for a more in-depth discussion of QEq.

A beneficial aspect of shielded Coulomb interactions is that the potential energy remains a convex function of the partial charges when interatomic distances become small. The QEq approach can be rightfully criticized for a variety of reasons, the most central ones being the following: partial charges are intrinsically ill-defined,[26–28] QEq produces hyperpolarizability[19,21,29] including a diverging dielectric constant in the thermodynamic limit,[30,31] fractional charges on isolated fragments,[18,32] and, most relevant to this work, the above-mentioned convexity of the potential energy in the partial charges is not necessarily established for the right reason.

Some issues related to the original treatment of shielded Coulomb interactions appear to have survived to this date. For example, the Streitz and Mintmire[17] potential in LAMMPS treats long-range interactions properly for the electrostatic interaction energies and forces of 1s-STOs, i.e., in `pair coul/streitz`, but it does not include these interactions for the partial charge calculations in the corresponding `fix qeq/slater`. Moreover, we have found that a follow-up[33] to the original QEq work[16] only appeared to be reproducible when shielding was used for the charge assignment but forces and energies were calculated using Coulomb interactions between point charges. In addition, the combination rule introduced in Ref. 33 for the orbital exponent, $\zeta_{ij}^{-1} = (\zeta_i/n_i + \zeta_j/n_j)$, where n_i and n_i are the principle quantum numbers of the valence electrons of atom i and j, respectively, lacks rigorous motivation and appears problematic when $n_i \neq 2$. In general, using STO shielding is prone to errors due to the analytical complexity. In fact, in quantum chemistry, it is quite common to replace STOs with Gaussian-type orbitals[34,35] as a basis set.

In this work, we explore the possibility to remedy many of the aforementioned issues by using Gaussian charge densities instead of ns-STOs, which also leads to quantitatively correct and convex Coulomb potentials. This is done in the context of QEq, because even the original QEq, despite all criticism, has benefits. It improves the accuracy of simulations compared to fixed-charge potentials, it can still be seen as appropriate for the simulation of conducting materials, e.g., electrodes, and last but not least, our work addresses merely the Coulomb interaction between atoms so that our results apply to any post-QEq method fixing the hyperpolarizability and related shortcomings of the original work. As such, the progress reported herein can also benefit any machine-learned potential[9,36,37] that is augmented with a post-QEq method. However, while the method presented is presumably not suitable for facilitating the training of such machine-learning force fields, it could provide an avenue for their efficient application. For the former, one could, for example, follow the strategy presented in Loche *et al.*,[38] which is based on PyTorch and JAX and relies on a framework for treating long-range many-body interactions in Huguenin-Dumittan *et al.*,[39] or, more generally, the strategy presented for HDNNPs in Tokita and Behler[40] It should be noted that, in principle, Gaussian charge densities, also in combination with QEq, can already be used in the Electrode implementation[13] in LAMMPS, and since this QEq implementation is based on that package, it benefits from a higher efficiency of the underlying particle-mesh implementation.[41] We note that others[37,42] also use a particle-mesh solver for very similar approaches. In an attempt to simplify QEq and make it more straightforward to use, while maintaining compatibility with previous QEq approaches, our method will be briefly introduced in the following.

THEORY AND METHODS

Charge equilibration

The total potential energy U can be divided into two parts, $U = U_0 + U_q$. Therein, U_0 encompasses all potential energy contributions that are not explicitly related to atomic partial charges. In turn, $U_q = U_{\mathrm{QEq}} + U_{\mathrm{coul}}$ includes all contributions associated with the N atomic charges $q_1, \ldots, q_N$ and can be further decomposed into the Coulomb energy U_{coul} and an energy term U_{QEq}, which reflects the chemical potential of the individual atoms. In QEq methods, the redox energy of each atom i is written as a Taylor series of at least second-order. Indeed, a second-order expansion of the redox energy as functions of the atomic charges is the most commonly applied approach,[14,15]

$$U_{\mathrm{QEq}}(\{q^N\}) \approx \sum_i^N \left(\chi_i q_i + \frac{1}{2} J_i^0 q_i^2\right), \tag{1}$$

where the QEq coefficients χ_i and J_i^0 are interpreted as the electronegativity and chemical hardness of the individual atomic species, respectively. The most commonly used approach to assessing the QEq coefficients relies on reproducing the ionization energy and electron affinity of the isolated atom.[43] While the chemical motivation of this choice is particularly obvious for describing metallic systems, the modeling of ionic systems may call for adapting the QEq coefficients to the underlying oxidation states.[44] To this end, one may also parameterize the overall interaction potential including the QEq coefficients in a concerted fit to best reproduce DFT benchmarks.[45,46] Returning to the derivation of the Coulomb energy, point charges would be a natural choice, as used in EEM, but this leads to issues such as infinite charge separation[44] (or polarization catastrophe[47]), resulting in non-physically high partial charges. To solve these problems, ns-STOs have been used.[16] As known from quantum mechanics, the use of ns-STOs as charge distributions

poses some challenges for the analytical and also numerical calculation of the Coulomb integral.[48] Thus, other more recent QEq implementations rely purely on Gaussians,[9,36,37] which have some advantages for evaluating overlap or Coulomb integrals and for use in efficient Ewald summation methods. Here, we describe all charges by Gaussians, which are normalized to the corresponding atomic partial charge q_i with the following expression:

$$\rho_i(\mathbf{r}) = q_i\left(\frac{\eta_i^2}{\pi}\right)^{3/2} \exp\left(-\eta_i^2|\mathbf{r}_i - \mathbf{r}|^2\right), \tag{2}$$

where η_i is a parameter that defines the width of the charge density. The Coulomb energy of such interacting Gaussians is calculated using a modified Ewald summation[49] for periodic systems,

$$\begin{aligned} U_{\text{coul}} = &\frac{1}{2}\sum_{i,j} q_i q_j \sum_{\mathbf{n}}{}' \frac{\operatorname{erfc}(\alpha|\mathbf{r}_{ij}+\mathbf{n}|) - \operatorname{erfc}(\eta_{ij}|\mathbf{r}_{ij}+\mathbf{n}|)}{|\mathbf{r}_{ij}+\mathbf{n}|} \\ &+ \frac{2\pi}{V}\sum_{i,j} q_i q_j \sum_{\mathbf{k}\neq 0} \mathrm{e}^{i\mathbf{k}\cdot\mathbf{r}_{ij}} \frac{1}{|\mathbf{k}|^2} \exp\left(-\frac{|\mathbf{k}|^2}{4\alpha^2}\right) \\ &- \frac{\alpha}{\sqrt{\pi}}\sum_i q_i^2 + \frac{1}{\sqrt{2\pi}}\sum_i \eta_i q_i^2, \end{aligned} \tag{3}$$

with V being the volume of the simulation box (assuming the usual tinfoil conditions for isotropic conducting systems[50]). Equation (3) is given in Gaussian units, as chosen in the remainder of this work. η_{ij} is calculated using the combination rule as follows:

$$\eta_{ij} = \frac{\eta_i \eta_j}{\sqrt{\eta_i^2 + \eta_j^2}}. \tag{4}$$

This combination rule results from the interaction of two Gaussian charge densities of width η_i and η_j in the Ewald summation and is adopted from the theoretical framework of the MetalWalls package.[51] In the Ewald approach, α is used to damp the Coulomb potential such that cutoff effects are reduced in the real-space summation. Accordingly, small α implies large real-space cutoff delimiters and vice versa. The first term in Eq. (3) describes hence the Coulomb energy of the auxiliary charges of width α and the correction of introducing the real-space Gaussian charge densities of width η_i as part of the model. The primed sum indicates that $\mathbf{n} = 0$ is skipped for $i = j$, i.e., the charges do not contribute to their own potential in the unit cell. The third term in Eq. (3) looks like a self-interaction, but this merely compensates for errors introduced in the Ewald summation from the reciprocal space in the second term, where interactions for $i = j$ are included for the auxiliary charges. The last term is the self-interaction of the real-space Gaussians. Using Eq. (3) to describe the Coulomb energy implies $\eta_i^2/2 > \alpha^2$,[49] defining a lower limit for the choice of η_i.

Merging the QEq and Coulomb sums, we can now write

$$U_q = U_{\text{QEq}} + U_{\text{coul}} = \sum_i \chi_i q_i + \frac{1}{2}\sum_{i,j} J_{ij} q_i q_j \tag{5}$$

as a matrix product with the vector $(q_1, \ldots, q_N)^T$. We define an effective hardness parameter,

$$J_{ii}^{\text{eff}} = J_i^0 + \sqrt{\frac{2}{\pi}}\eta_i, \tag{6}$$

as a diagonal element of the matrix $\mathbf{J}$ in the limiting case of non-interacting, infinitely separated particles [*cf.* Eq. (8) of Vondrák *et al.*[36]] The effective hardness J_{ii}^{eff} is, therefore, greater than the chemical hardness J_i^0, which must be adjusted according to the choice of η_i. A common choice for this is to set $J_{ii}^{\text{eff}} = \sqrt{2/\pi}\,\eta_i$, i.e., $J_i^0 = 0$.[52,53] Note that the choice of η_i has a significant impact on the partial charges. In applications of the QEq for ML force fields, the hardness is often written as a sum of non-classical (e.g., exchange–correlation) contribution and a classical electrostatic term.[9,36,54] In this terminology, $\sqrt{2/\pi}\eta_i$ is the classical term, i.e., the self-interaction, and the non-classical term can be positive or is simply set to zero.[54]

Finally, to obtain the equilibrium atomic charges, the electrostatic energy must be minimized with respect to the charges q_i and one arrives at an expression that is very similar to that found in Electrode,[41]

$$\frac{\partial U_q}{\partial q_i} = \chi_i + \sum_j J_{ij} q_j = 0, \tag{7}$$

while the total system charge is constrained to a constant $q_{\text{tot}} = \sum_i q_i$ and is typically zero. The constraint could be enforced using the method of Lagrange multipliers[16] or by employing a projection matrix.[55,56] The set of linear equations defined by Eq. (7) along with the constraint is here solved for the charges using the conjugate gradient (CG) method.

Choice of hardness and Gaussian width

A prerequisite for QEq is that the energy as a function of charges has a minimum. This is the case if the matrix of Coulomb interactions $\mathbf{J}$ is positive-definite. However, depending on the choice of the hardness and the screening parameters between atoms, this might not be the case. If $\mathbf{J}$ is not positive-definite, algorithms for the minimization may yield a saddle point or not converge at all. This issue is well known in QEq and especially relevant for small atom distances.[24,44,47] Here, we illuminate the cause of the issue and show how it can be avoided for a system of Gaussian-shaped charges.

In order to illustrate the issue, we consider a system of two atoms at a distance r_{12} without periodic boundary conditions. In this case, the symmetric matrix $\mathbf{J} \in \mathbb{R}^{2\times 2}$ is positive-definite if

$$J_{12}^2 < J_{11} J_{22}. \tag{8}$$

If described as point charges, the non-diagonal element of $\mathbf{J}$ is $J_{12} = r_{12}^{-1}$. This interaction diverges for small distances, and thus, the hardnesses have to be chosen such that Eq. (8) is fulfilled for all distances that may occur during a simulation. The situation is different for two Gaussian charges. Here, the non-diagonal element is $J_{12} = \operatorname{erf}(\eta_{12} r_{12})/r_{12}$ and does not diverge but has a maximum at zero: $\lim_{r_{12}\to 0} J_{12}(r_{12}) = 2\eta_{12}/\sqrt{\pi}$. In the constant potential method (CPM), the diagonal elements are set to the self-interaction of Gaussians in Eq. (3), which is the limit for $r_{ij} \to 0$ with $\eta_i = \eta_j$. This choice ensures that Eq. (8) is true for all values $r_{12} > 0$, i.e., the matrix is positive-definite by design in the CPM. If the self-interactions on the diagonal are replaced by hardness parameters, a choice of

$$\eta_i \leq \sqrt{\frac{\pi}{2}} J_{ii} \tag{9}$$

will ensure that the matrix is positive definite and vice versa for this simple system. For a given screening parameter η_i, a hardness can be set, which fulfills this equation. This simple example with two atoms shows that the hardness and screening parameters for QEq have to be chosen with care, either by fulfilling Eq. (9) or by ensuring that distances during a simulation are large, resulting in small interactions relative to the hardnesses. For more than two atoms, Eq. (8) is a necessary but not a sufficient criterion for the positive definiteness of **J**. One can check whether the smallest eigenvalue of **J** is larger than zero, to ensure it is positive-definite.[56]

Charge equilibration parameters

First, to demonstrate the behavior of our QEq implementation in the limit of EEM, the results are compared with the previously published data of a Ti/TiO_x system.[58] Second, SiO_2 polymorphs such as α-quartz, stishovite, and amorphous silica have previously been successfully described by a combination of QEq and a Morse potential,[33] making this potential an ideal test candidate against which to further compare our method.

While the QEq parameters for SiO_2 are physically motivated and discussed in more detail in the underlying publication by Rappé and Goddard,[16] empirically derived parameters are often used for more complex molecular simulations. This is the case for Ti/TiO_x, where the EEM parameters were obtained by Schneider and Ciacchi[57] such that the partial charges are proportional to the Bader charges and consistent with the Matsui and Akaogi[59] charges and biomolecular force fields.

The form of the short-range potential for SiO_2 is defined in Ref. 33 as

$$U_{ij} = D_0\left[e^{-2\gamma(r_{ij}-r_0)} - 2e^{-\gamma(r_{ij}-r_0)}\right], \tag{10}$$

where D_0 is the bond strength, r_0 is the bond length at equilibrium, and γ is an inverse length parameter that defines how sharp the potential is around the equilibrium bond distance. The parameters for Si–O, O–O, and Si–Si have not been modified and can be found in the original publication of Demiralp *et al.*[33] Electronegativities χ and atomic hardnesses J^{eff} used here for Si and O are summarized in Table I. Similarly to the original work, the Morse interaction is truncated at 9 Å. Coulomb interactions for SiO_2 were calculated using the above introduced Ewald summation, which explicitly includes the interaction between real-space Gaussians, with a real-space cutoff of 12 Å and an accuracy setting of 10^{-6}. Since Gaussians with a width of η are used instead of ns-STOs, a simple strategy is provided to convert them, described later in the text, and the resulting values are given in Table I. The integration time step for the numerical solution of Newton's equation of motion has been set to 1 fs in all molecular dynamics (MD) simulations, unless otherwise noted. Standard couplings of 100 time steps were used for the thermostat in both the *NVT* and *NpT* simulations, and a coupling of 1000 time steps was used in the case of the barostat.

The stishovite structure contained 3840 atoms and was created from a $8 \times 8 \times 10$ repeated unit cell with cell dimensions of $a = b = 4.18$ Å and $c = 2.67$ Å, which corresponds to a density of 4.28 g/cm^3. α-quartz has been obtained from a $3 \times 3 \times 3$ repeated orthorhombic cell of dimensions $a = 9.83$ Å, $b = 8.51$ Å, and $c = 10.80$ Å containing totally 1944 atoms, which corresponds to a density of 2.65 g/cm^3. Amorphous silica was produced by a melt-quenching process explained in more detail later in the corresponding chapter.

TABLE I. QEq parameters for SiO_2 and Ti/TiO_x. χ and J^{eff} parameters for Ti/TiO_x were taken from Schneider and Ciacchi[57] and for SiO_2 from Demiralp *et al.*,[33] respectively. η is obtained from a fit to the Coulomb energies shown in Fig. 3 and explained in the main text.

	`QEq/electrode` parameters for SiO_2		
	χ (V)	J^{eff} (V/e)	η (Å^{-1})
Si	4.168	6.974	0.474
O	8.741	13.364	0.834
	`QEq/electrode` parameters for Ti/TiO_x		
	χ (V)	J^{eff} (V/e)	
Ti	0.0	12.864	
O	8.729	17.197	

The Ti/TiO_x slab in Schneider and Ciacchi[57] was generated by the incorporation of O_2 molecules into a periodically repeated $(2\sqrt{3} \times 3)$ surface supercell consisting of five Ti(0001) layers of atoms in the *xy* plane. It has also been extended in the z-direction by a mirroring operation (*cf.* Fig. 1), as only one side was oxidized. Further details on how the oxidized interface was obtained can be found in the corresponding papers.[57,58] The system used here is a 2×2 repeated cell of the original oxidized slab in the plane direction. For Ti/TiO_x, a 10 Å cutoff is used for the real-space part of the electrostatic interactions. QEq parameters for Ti/TiO_x are summarized in Table I. For Ti/TiO_x, we do not provide η because we will show that if we choose a sufficiently large η, i.e., sufficiently narrow Gaussians, we converge to the EEM results.

RESULTS

Oxidized titanium surface

We begin with the analysis of the Ti/TiO_x slab, as this is an interesting test case to study the QEq approach in the point charge limit. The given parameters for Ti and O were optimized by Schneider and Ciacchi[57] to reproduce the Matsui and Akaogi[59] fixed charges of bulk rutile. It has been shown that these EEM parameters give reasonable charges for partially oxidized Ti atoms in the slab and are in good agreement with their *ab initio* results.

Parameters mentioned in Table I are used for the here performed QEq calculations with varying Gaussian widths. Note that only zero step calculations were performed to obtain just the partial charges and atoms did not move, i.e., no MD steps were performed. In principle, one should obtain the EEM partial charges by using large values for η_i, i.e., very narrow Gaussians. Conversely, this means that in this case, electrostatic interactions are described purely by point charge interactions. While $\operatorname{erfc}(\eta_{ij}|\mathbf{r}_{ij} - \mathbf{n}|)$ in Eq. (3) goes to zero for very narrow Gaussians and is otherwise skipped in the sum for the case of $i = j$ and $\mathbf{n} = 0$, the self-interaction term from the interaction between real-space Gaussians $U_{\text{self}} = (2\pi)^{-1/2}\sum_i \eta_i q_i^2$ goes to infinity. To avoid this problematic self-interaction of the Gaussians, this interaction is implicitly included in the hardness,

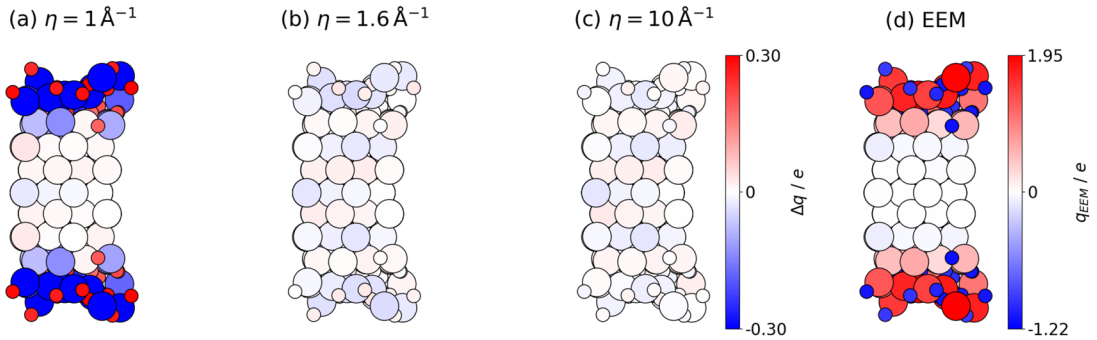

FIG. 1. Charges, q, for Ti/TiO_x obtained with EEM (d) and charge differences, $\Delta q = q_{EEM} - q_{QEq}$, from EEM and QEq, respectively, using different Gaussian widths (a)–(c). Ti atoms are represented with a larger sphere than O atoms.

cf. Eq. (6), and J_{ii}^{eff} is the user-defined constant hardness parameter. In Fig. 2, the minimum eigenvalues of the matrix **J** are plotted as a function of η. The smallest eigenvalues using different hardness settings all converge for $\eta > 1.60$ Å^{-1}. In Figs. 1(a)–1(c), the charge differences Δq between QEq and EEM are shown for $\eta = 1.0$, 1.6, and 10.0 Å^{-1}. The maximum charge difference is between 0.025 and −0.030 e already for $\eta = 10$ Å and is found close to the surface. This nicely illustrates that if the Gaussians are small enough, the EEM charges are, indeed, obtained with negligible differences.

Silicon dioxide polymorphs

There have been several attempts to model SiO_2 polymorphs, including silicon and silica interfaces, with QEq approaches.[33,60–62] However, it is often unclear whether the long-range electrostatic interactions are calculated and treated consistently in the various steps, i.e., the derivation of the partial charges and the subsequent Ewald summation, or whether some parts are tapered to avoid costly computations. While it is not entirely clear whether long-range interactions were treated consistently in the partial charge calculation as well as in the final electrostatic calculations in Demiralp *et al.*[33] and van Duin *et al.*,[60] it appears that Fogarty *et al.*[61] used a QEq variant with a taper function (*cf.* the `SERIALREAX` implementation of Aktulga *et al.*[63] for LAMMPS) that neglects important long-range interactions and, moreover, uses only 1s-STOs for the partial charge calculations instead of the correct 3s-STO and 2s-STO for Si and O, respectively.

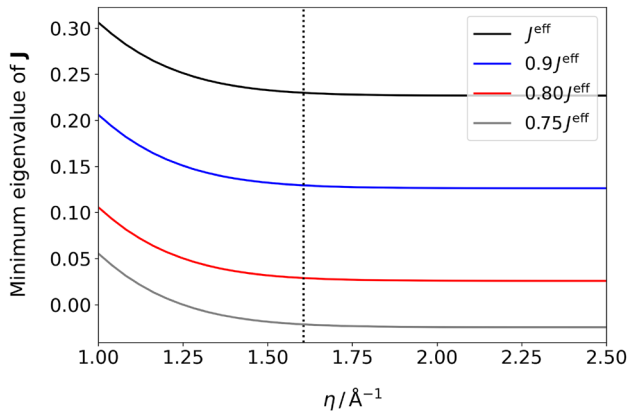

FIG. 2. Minimum eigenvalues of the matrix **J** with different η and different hardnesses J^{eff}. The black curve corresponds to the QEq parameters for Ti and O given in Table I with the effective hardness equal to J_{Ti}^0 and J_{O}^0, respectively. The blue, red, and gray curves correspond to arbitrarily decreasing values of the effective hardnesses. The black dashed line indicates the point where the minimum eigenvalue approximately converges for all hardness settings.

In the following, we will try to reproduce the results of Demiralp *et al.*,[33] but instead of using *n*s-STOs, we will use Gaussians. To switch from *n*s-STOs to Gaussians, i.e., $(n, \zeta) \rightarrow \eta$, we fitted the Coulomb energies from the two-electron Coulomb repulsion of two atomic species (i.e., between Si and Si or O and O) using Gaussians instead of using *n*s-STOs. In general, the Coulomb energy between two charge distributions ρ_i and ρ_j at positions r and r', respectively, is defined as

$$U_{ij} = \int_{\mathbb{R}^3} \mathrm{d}^3 r \int_{\mathbb{R}^3} \mathrm{d}^3 r' \frac{\rho_i(\mathbf{r})\rho_j(\mathbf{r}')}{|\mathbf{r} - \mathbf{r}'|}. \tag{11}$$

Plugging Eq. (2) into Eq. (11) and using $r = |\mathbf{r}_i - \mathbf{r}_j|$ with some algebra gives the Coulomb energy between two Gaussians separated by the distance r,

$$U_{ij}(r) = e^2 \frac{\operatorname{erf}(\eta_{ij} r)}{r}. \tag{12}$$

In Figs. 3(a) and 3(b), the Coulomb energies using η_{Si} and η_{O}, obtained from a non-linear fit using the Levenberg–Marquardt algorithm of the energies from Eq. (12) to corresponding energies using *n*s-STOs, are shown. The resulting fitted values are $\eta_{\text{Si}} = 0.474$ Å^{-1} and $\eta_{\text{O}} = 0.836$ Å^{-1}. The corresponding two-center Coulomb integrals of *n*s-STOs in Fig. 3 are calculated using the method of Ref. 20.

There is some discrepancy in the way the QEq parameters for Si–O are obtained when comparing Demiralp *et al.*[33] and Rappe and Goddard.[16] While in both studies the radius of the atom in the standard state, R_A, is the same and is used to obtain the orbital exponent for the *n*s-STO, in Demiralp *et al.*,[33] a combination rule is introduced to calculate the orbital exponent ζ_{AB} of the Slater orbital, but

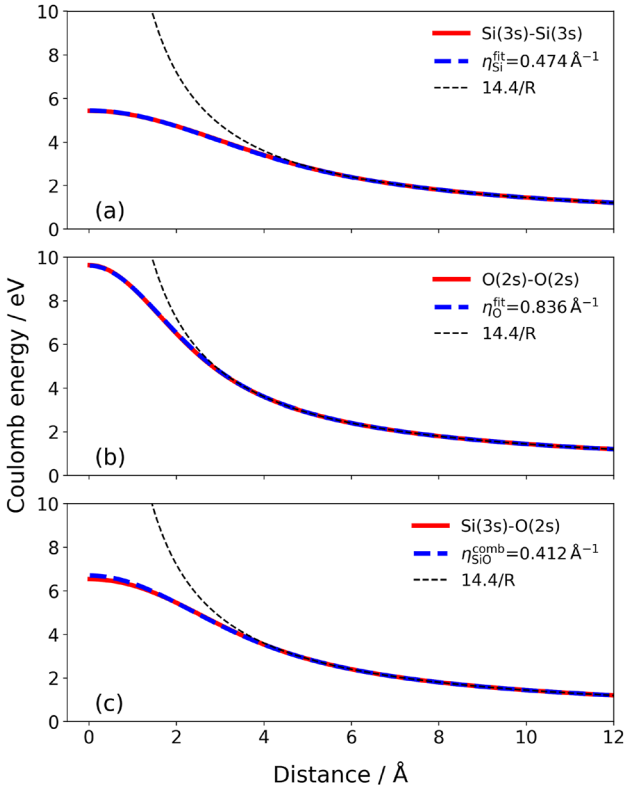

FIG. 3. Non-linear least square fit of Coulomb energies from Gaussians to the results of two interacting *n*s-STOs for Si–Si and O–O. Energies for interacting Gaussians between Si and O are obtained using the combination rule in Eq. (4).

this does not reproduce the ζ_A values mentioned in Rappe and Goddard[16] if we substitute the corresponding values for ζ_{AB}, i.e., $\zeta_{SiSi} \neq \zeta_{Si}$ and $\zeta_{OO} \neq \zeta_{O}$. In addition, in that formulation, a mixing parameter for the principal quantum number for Si and O is required but is missing. It is not clear why a combination rule is needed at all. The Coulomb potential presented in Rappe and Goddard[16] actually does not need it, since both orbitals for Si and O should appear there separately if $\rho_1 = |\phi_{Si}|^2$ and $\rho_2 = |\phi_{O}|^2$, where ϕ_{Si} and ϕ_{O} are the corresponding *n*s-STOs [*cf.* Eq. (11)].

The QEq interaction between Si and O shown in Fig. 3(c) is described here by η_{SiO} and is obtained by using the combination rule for two different Gaussians given in Eq. (4). This gives $\eta_{SiO}^{comb} = 0.412 Å^{-1}$ and yields Coulomb energies very similar to the energy from a Coulomb integral between a 3s-STO for silicon and a 2s-STO for oxygen and the corresponding Slater exponents ζ as given in Rappe and Goddard.[16] Note that using the above combination rule for Gaussians, $\eta_{ii} \neq \eta_i$, and the conversion is $\eta_i = \eta_{ii}/\sqrt{2}$ (for a derivation of the combination rule and this expression, we refer to the Ewald theory presented in Refs. 51 and 56.)

In an effort to reproduce the structural properties of stishovite and quartz, it is interesting to note that Demiralp *et al.*[33] do not seem to use short-range correction terms for the interaction of *n*s-STOs in their work, at least not in the force calculations, since only without these similar densities could be obtained. As a side note, such correction terms for 1s-STO have been previously introduced by Nakano[64] but are seldomly implemented. Neglecting short-range corrections due to Coulomb shielding results in an Ewald summation equivalent to that of point charges (assuming the self-interaction term is included in the hardness or set to zero). Ignoring Gaussians and instead using point charges to calculate forces and energies, the density for α quartz and stishovite was 2.55 and 4.29 g/cm^3, respectively. While these densities agree reasonably with those reported in Demiralp *et al.*,[33] the use of Gaussian charges in the force and energy calculations decreased the densities and resulted in 2.49 g/cm^3 for α-quartz and 3.68 g/cm^3 for stishovite. The stronger decrease in density of stishovite could be explained due to the stronger repulsion of Gaussians than point charges as in stishovite, atoms are closer together than in α-quartz and silica. It should be stressed again that in both cases, the computation of the partial charges is using Gaussians (instead of *n*s-Slater orbitals or simple point charges), but the way the forces and energies are calculated differs, i.e., using a simple point charge model or by including the full Gaussian interactions through the correction terms introduced in the Ewald summation of Eq. (3).

Structural properties of silica depend on the melting and quenching procedure[65] and in particular on the quenching rate, e.g., quenching rates of 12.5, 25.0, and 50.0 K/ps using STOs resulted in different silica densities of 2.32, 2.33, and 2.35 g/cm^3.[33] Here, the amorphous silica was generated by following as closely as possible the recipe presented in Demiralp *et al.*[33] We start by melting a β-cristobalite crystal structure. The initial structure had a lattice constant of 7.40 Å and was repeated 3 × 3 × 3, thus containing 1536 atoms with a density of 1.97 g/cm^3. The crystal structure was annealed at 4000 K for 200 ps instead of the 40 ps mentioned in Demiralp *et al.*[33] to remove any remnants of the β-cristobalite crystal structure. The time step was set to 0.5 fs to ensure the stability of the simulation. Then, the system was cooled using *NVT* dynamics by decreasing the temperature at a rate of 25.0 K/ps to 1000 K. At 1000 K, we switched to *NpT* dynamics and continued cooling at the same rate to 300 K. After quenching, constant pressure relaxation was performed at 300 K and 1 atm for 1.5 ns and the silica obtained had a density of 2.19 g/cm^3, very close to the experimental densities, which are typically around 2.20 g/cm^3.[66]

Somewhat unexpectedly, the density for silica differed from the results of Demiralp *et al.*,[33] although we followed the recipe as closely as possible. Most importantly, we use (fitted) Gaussians instead of *n*s-STO, which might explain some differences. Another explanation is that some details of the simulation parameters and settings were not given, e.g., coupling constants to the barostat and thermostat, so we used commonly used ones. To shed more light on this and to see if other structural details are affected, the radial pair and angle distributions in amorphous silica were examined to see if there were other structural differences. The effect of using a point charge or a Gaussian charge model on the structural results was also investigated.

The O–Si–O bond angle distributions differ between the use of point charges and Gaussian charges. Both are shown for comparison in Fig. S3. Nevertheless, the mean differences are small compared to the results found in Demiralp *et al.*[33] and experimental results. The mean O–Si–O angle was determined here to be 109° ± 9° and is similar to that found in Demiralp *et al.*,[33] and by neutron diffraction, an angle of 109.4°[67] was found.

Si–O–Si angle distributions from melt-quench simulations using Gaussians or point charges in the force and energy calculations are shown in Fig. 4. The average Si–O–Si angle when using point charges agreed well to that observed in nuclear magnetic resonance (NMR) spectroscopy of 146.7°.[69] However, when using Gaussians in the force and energy computations, an average Si–O–Si angle of 118° ± 18° was found, which is significantly smaller than that obtained by using point charges. In the case of Si–O–Si, a rather large fraction of angles around 90° were also observed, as shown in Fig. 4, regardless of whether Gaussian or point charges were used but less pronounced in the case of point charges. Interestingly, the appearance of these 90° angles correlates with the increased undercoordination of the Si atoms. Unfortunately, the data for Si–O–Si were not shown in Demiralp *et al.*[33] to compare whether these angles occur there as well. Table II summarizes the mass densities, radial distribution functions (RDFs), and mean angles of amorphous silica for the case of Gaussians, point charges, and experimental data for comparison. Apart from this, with respect to partial atomic charges, there is good agreement with charges found in Demiralp *et al.*[33] Here, using Gaussians instead of *n*s-STOs, average partial charges of $\langle q_{Si} \rangle = 1.30\ e$ and $\langle q_O \rangle = -0.65\ e$ for *α*-quartz, $\langle q_{Si} \rangle = 1.33\ e$ and $\langle q_O \rangle = -0.67\ e$ for stishovite, and $\langle q_{Si} \rangle = 1.28\ e$ and $\langle q_O \rangle = -0.64\ e$ for amorphous silica have been obtained. A summary of obtained partial charges and densities for the SiO_2 polymorphs is given in Table S1.

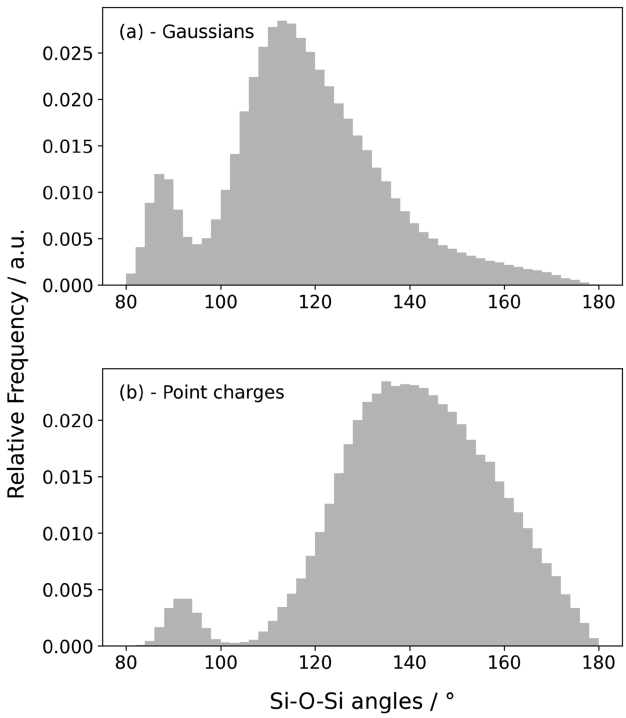

FIG. 4. Si–O–Si angle distribution of am-SiO_2 generated by a melt-quenching process using the Morse potential for non-electrostatic interactions and QEq with (a) Gaussian charges and (b) point charges.

TABLE II. Structural data for amorphous SiO_2 from melt-quench simulations using our QEq implementation.

	Gaussians	Point charges	Experimental
Density (g/cm^3)	2.19	2.14	2.20[a]
Si–O–Si angle (°)	118 (18)	141 (18)	144 (38),[a] 153[b]
O–Si–O angle (°)	109 (9)	109 (7)	109.4,[b] 109.5[a]
Si–O RDF first max. (Å)	1.7	1.62	1.608,[c] 1.620[a]
Si–O first min.	2.18	2.22	...
Si–O second max.	4.26	4.18	4.15[a]
O–O RDF first max.	2.78	2.62	2.626,[c] 2.65[a]
Si–Si RDF first max.	2.98	3.14	3.12[a]

[a]Reference 66.
[b]Reference 67.
[c]Reference 68.

DISCUSSION AND OUTLOOK

In this work, we presented a QEq formulation where the charge densities are described by real-space Gaussians. Both Coulomb and QEq terms are calculated using a long-range solver, i.e., the Ewald summation, taking correctly into account real-space charge distributions. Three parameters are required for this: the electronegativity, the hardness, and the reciprocal width η_i of the charge density. Optimized widths were obtained by fitting the Coulomb energy of two isolated Gaussian charge distributions to the repulsion between STOs and applied to the case study of SiO_2 polymorphs.

We have also studied the convergence of our algorithm in terms of different settings for the hardness and Gaussian widths. The Coulomb matrix needs to be positive definite for the QEq algorithm to converge. We first showed this for a simple example of two interacting Gaussians. We have studied this also for a more complex system by calculating the minimum eigenvalue of the Coulomb matrix for different QEq settings on the example of Ti/TiO_x. In the limit of very narrow Gaussians, we were able to show that our algorithm converges to EEM results. By studying the dependence of the Coulomb matrix on the effective hardness and the width of the Gaussian, we found that for a reasonable hardness choice, Gaussians can be made almost point-like.

Although we obtain very reasonable partial charges for SiO_2 polymorphs, the densities of SiO_2 polymorphs previously obtained in Demiralp *et al.*[33] are reproducible only if we neglect the additional force correction in the Ewald summation due to the Gaussians interacting at short distances. While the densities for *α*-quartz, stishovite, and silica are in agreement with experimental densities using the approach presented here, a higher density was found for amorphous silica in the original work by Demiralp *et al.*[33] It should be noted that we do not get exactly the experimental values, nor the values mentioned in Demiralp. One reason could be that the (re)fitted Gaussians do not exactly reproduce the STO behavior originally used. The density found for silica depends on many factors, e.g., the exact protocol of the simulations or the manufacturing process of real specimens, but experimentally, it is usually around 2.20 g/cm^3.[66] The inclusion of Gaussian interactions in the forces and energies also had a strong effect on O–Si–O and an even stronger effect on the Si–O–Si angle distributions. Notably, if we use point charges for the computation of forces and energies, while still using

Gaussians for the charge assignment, the resulting silica structure agrees much better, in terms of structural properties such as bond lengths and bond angles, despite a somewhat lower density of 2.14 g/cm^3. In conclusion, the results presented here suggest a reparameterization of the Ref. 33 potential, which is beyond the scope of this work as we focus more on the general aspects of QEq methods and their implementation, but is important for follow-up work on Si/SiO_x interfaces.

The simple recipe to switch from *n*s-STO to Gaussians by doing a fit as shown in Fig. 3 should be emphasized here again. One could think of setting the effective hardness completely to the self-interaction from the fit, but this has a caveat. Apparently, the hardness J^0 from the literature for SiO_2 and TiO_2 (we even tested NaCl) is always larger than the self-interaction of Gaussians using η obtained from the fit of Fig. 3. Since J^0 is often calculated from the experimental idempotential and electron affinity, other quantum chemical effects are included, e.g., exchange–correlation and a fit to Coulombic energies where such information is neglected are expected to give lower values for the hardness. Thus, setting $J_i^0 = 0$ should be done with care.

Our implementation has, moreover, some advantages due to its flexibility and many other interesting features. For example, due to the similarity of QEq to the CPM method of the ELECTRODE package, our QEq implementation as such allows for interactions between Gaussians and point charges. This is needed, for example, whenever QEq is used in combination with water models with fixed point charges. It would also allow the consideration of long-range interactions in Streitz and Mintmire[17] partial charge calculations, since the effective nuclear charges are described by point charges.

SUPPLEMENTARY MATERIAL

The supplementary material provides additional details on the structural differences between the use of Gaussian and point charges in the QEq formalism: A table summarizing the average charges and densities for different SiO_2 polymorphs, the coordination numbers and radial distributions of Si and O, and the angular distributions of O–Si–O is also provided.

ACKNOWLEDGMENTS

We acknowledge the scientific exchange and support of the research initiative BlueMat: Water-Driven Materials, Hamburg (Germany). This work was funded by the Deutsche Forschungsgemeinschaft (DFG, German Research Foundation), Grant Nos. 192346071, 390794421, 525597740, and 529997859.

AUTHOR DECLARATIONS

Conflict of Interest

The authors have no conflicts to disclose.

Author Contributions

Kamila Savvidi: Conceptualization (equal); Formal analysis (equal); Investigation (equal); Methodology (equal); Software (equal); Validation (equal); Writing – original draft (equal); Writing – review & editing (equal). **Ludwig Ahrens-Iwers**: Conceptualization (supporting); Formal analysis (supporting); Methodology (equal); Validation (equal); Writing – original draft (supporting); Writing – review & editing (equal). **Lucio Colombi Ciacchi**: Methodology (supporting); Resources (equal); Validation (supporting); Writing – review & editing (supporting). **Dirk Zahn**: Conceptualization (supporting); Methodology (supporting); Validation (equal); Writing – review & editing (supporting). **Martin H. Müser**: Conceptualization (supporting); Formal analysis (supporting); Investigation (supporting); Methodology (equal); Supervision (supporting); Writing – original draft (equal); Writing – review & editing (equal). **Robert Horst Meißner**: Conceptualization (equal); Data curation (equal); Formal analysis (equal); Funding acquisition (equal); Investigation (equal); Methodology (equal); Project administration (equal); Resources (equal); Software (equal); Supervision (equal); Validation (equal); Writing – original draft (equal); Writing – review & editing (equal).

DATA AVAILABILITY

The data that support the findings of this study are available from the corresponding author upon reasonable request.

REFERENCES

[1] M. P. Allen and D. J. Tildesley, *Computer Simulation of Liquids*, 2nd ed. (Oxford University Press, Oxford, 2017).
[2] D. Frenkel and B. Smit, *Understanding Molecular Simulation: From Algorithms to Applications*, 2nd ed. (Academic Press, San Diego, 2001).
[3] J. A. Harrison, J. D. Schall, S. Maskey, P. T. Mikulski, M. T. Knippenberg, and B. H. Morrow, Appl. Phys. Rev. **5**, 031104 (2018).
[4] M. H. Müser, S. V. Sukhomlinov, and L. Pastewka, Adv. Phys.: X **8**, 2093129 (2022).
[5] R. Car and M. Parrinello, Phys. Rev. Lett. **55**, 2471 (1985).
[6] D. Marx and J. Hutter, "Ab initio molecular dynamics: Theory and implementation," in *Modern Methods and Algorithms of Quantum Chemistry*, edited by J. Grotendorst (John von Neumann Institute for Computing, 2009), pp. 301–449.
[7] J. Behler, J. Chem. Phys. **145**, 170901 (2016).
[8] V. L. Deringer, M. A. Caro, and G. Csányi, Adv. Mater. **31**, 1902765 (2019).
[9] T. W. Ko, J. A. Finkler, S. Goedecker, and J. Behler, Nat. Commun. **12**, 398 (2021).
[10] W. B. Dapp and M. H. Müser, J. Chem. Phys. **139**, 064106 (2013).
[11] H. G. Lee, S. Y. Kim, and J. S. Lee, npj Comput. Mater. **8**, 103 (2022).
[12] T. Liang, A. C. Antony, S. A. Akhade, M. J. Janik, and S. B. Sinnott, J. Phys. Chem. A **122**, 631–638 (2018).
[13] L. J. V. Ahrens-Iwers, M. Janssen, S. R. Tee, and R. H. Meißner, J. Chem. Phys. **157**, 084801 (2022).
[14] W. J. Mortier, K. Van Genechten, and J. Gasteiger, J. Am. Chem. Soc. **107**, 829 (1985).
[15] W. J. Mortier, S. K. Ghosh, and S. Shankar, J. Am. Chem. Soc. **108**, 4315–4320 (1986).
[16] A. K. Rappe and W. A. Goddard III, J. Phys. Chem. **95**, 3358 (1991).
[17] F. H. Streitz and J. W. Mintmire, Phys. Rev. B **50**, 11996–12003 (1994).
[18] S. W. Rick, S. J. Stuart, and B. J. Berne, J. Chem. Phys. **101**, 6141–6156 (1994).
[19] R. Chelli, P. Procacci, R. Righini, and S. Califano, J. Chem. Phys. **111**, 8569–8575 (1999).
[20] R. A. Nistor, J. G. Polihronov, M. H. Müser, and N. J. Mosey, J. Chem. Phys. **125**, 094108 (2006).

[21] P. T. Mikulski, M. T. Knippenberg, and J. A. Harrison, J. Chem. Phys. **131**, 241105 (2009).
[22] T. Verstraelen, P. W. Ayers, V. Van Speybroeck, and M. Waroquier, J. Chem. Phys. **138**, 074108 (2013).
[23] I. Leven and T. Head-Gordon, J. Phys. Chem. Lett. **10**, 6820–6826 (2019).
[24] D. Ongari, P. G. Boyd, O. Kadioglu, A. K. Mace, S. Keskin, and B. Smit, J. Chem. Theory Comput. **15**, 382–401 (2019).
[25] F. Jensen, J. Chem. Theory Comput. **19**, 4047–4073 (2023).
[26] K. B. Wiberg and P. R. Rablen, J. Comput. Chem. **14**, 1504–1518 (1993).
[27] J. Meister and W. H. E. Schwarz, J. Phys. Chem. **98**, 8245–8252 (1994).
[28] I. Choudhuri and D. G. Truhlar, J. Chem. Theory Comput. **16**, 5884–5892 (2020).
[29] G. Lee Warren, J. E. Davis, and S. Patel, J. Chem. Phys. **128**, 144110 (2008).
[30] R. A. Nistor and M. H. Müser, Phys. Rev. B **79**, 104303 (2009).
[31] T. Verstraelen, S. V. Sukhomlinov, V. Van Speybroeck, M. Waroquier, and K. S. Smirnov, J. Phys. Chem. C **116**, 490–504 (2011).
[32] J. Chen and T. J. Martínez, Chem. Phys. Lett. **438**, 315–320 (2007).
[33] E. Demiralp, T. Çağin, and W. A. Goddard, Phys. Rev. Lett. **82**, 1708–1711 (1999).
[34] W. J. Hehre, R. F. Stewart, and J. A. Pople, J. Chem. Phys. **51**, 2657–2664 (1969).
[35] P. M. W. Gill and J. A. Pople, Int. J. Quantum Chem. **40**, 753–772 (1991).
[36] M. Vondrák, K. Reuter, and J. T. Margraf, J. Chem. Phys. **159**, 054109 (2023).
[37] M. Gubler, J. A. Finkler, M. R. Schäfer, J. Behler, and S. Goedecker, J. Chem. Theory Comput. **20**, 7264 (2024).
[38] P. Loche, K. K. Huguenin-Dumittan, M. Honarmand, Q. Xu, E. Rumiantsev, W. B. How, M. F. Langer, and M. Ceriotti, "Fast and flexible long-range models for atomistic machine learning," J. Chem. Phys. **162**(14), 142501 (2025).
[39] K. K. Huguenin-Dumittan, P. Loche, N. Haoran, and M. Ceriotti, J. Phys. Chem. Lett. **14**, 9612–9618 (2023).
[40] A. M. Tokita and J. Behler, J. Chem. Phys. **159**, 121501 (2023).
[41] L. J. V. Ahrens-Iwers and R. H. Meißner, J. Chem. Phys. **155**, 104104 (2021).
[42] L. Zeng, T. Wu, T. Ye, T. Mo, R. Qiao, and G. Feng, Nat. Comput. Sci. **1**, 725 (2021).
[43] R. G. Parr and R. G. Pearson, J. Am. Chem. Soc. **105**, 7512 (1983).
[44] C. E. Wilmer, K. C. Kim, and R. Q. Snurr, J. Phys. Chem. Lett. **3**, 2506 (2012).
[45] J. D. Gale, J. Chem. Soc., Faraday Trans. **93**, 629–637 (1997).
[46] J. D. Gale and A. L. Rohl, Mol. Simul. **29**, 291–341 (2003).
[47] S. Naserifar, D. J. Brooks, W. A. Goddard, and V. Cvicek, J. Chem. Phys. **146**, 124117 (2017).
[48] S. F. Boys, "Electronic wave functions—I. A general method of calculation for the stationary states of any molecular system," Proc. R. Soc. London, Ser. A **200**, 542–554 (1950).
[49] T. R. Gingrich and M. Wilson, Chem. Phys. Lett. **500**, 178–183 (2010).
[50] I.-C. Yeh and M. L. Berkowitz, J. Chem. Phys. **111**, 3155–3162 (1999).
[51] A. Marin-Laflèche, M. Haefele, L. Scalfi, A. Coretti, T. Dufils, G. Jeanmairet, S. Reed, A. Serva, R. Berthin, C. Bacon, S. Bonella, B. Rotenberg, P. Madden, and M. Salanne, J. Open Source Software **5**, 2373 (2020).
[52] H. Nakano and H. Sato, J. Chem. Phys. **151**, 164123 (2019).
[53] S. Bi and M. Salanne, ACS Nano **16**, 18658 (2022).
[54] C. G. Staacke, S. Wengert, C. Kunkel, G. Csányi, K. Reuter, and J. T. Margraf, Mach. Learn.: Sci. Technol. **3**, 015032 (2022).
[55] M. H. Shariff, Comput. Math. Appl. **30**, 25 (1995).
[56] T. Gingrich, "Simulating surface charge effects in carbon nanotube templated ionic crystal growth," M.S. thesis, University of Oxford, Oxford, 2010.
[57] J. Schneider and L. C. Ciacchi, Surf. Sci. **604**, 1105–1115 (2010).
[58] J. Schneider and L. C. Ciacchi, J. Chem. Theory Comput. **7**, 473 (2011).
[59] M. Matsui and M. Akaogi, Mol. Simul. **6**, 239–244 (1991).
[60] A. C. T. van Duin, A. Strachan, S. Stewman, Q. Zhang, X. Xu, and W. A. Goddard, J. Phys. Chem. A **107**, 3803–3811 (2003).
[61] J. C. Fogarty, H. M. Aktulga, A. Y. Grama, A. C. T. van Duin, and S. A. Pandit, J. Chem. Phys. **132**, 174704 (2010).
[62] T.-R. Shan, B. D. Devine, J. M. Hawkins, A. Asthagiri, S. R. Phillpot, and S. B. Sinnott, Phys. Rev. B **82**, 235302 (2010).
[63] H. M. Aktulga, J. C. Fogarty, S. A. Pandit, and A. Y. Grama, Parallel Comput. **38**, 245–259 (2012).
[64] A. Nakano, Comput. Phys. Commun. **104**, 59–69 (1997).
[65] N. T. Huff, E. Demiralp, T. Çağin, and W. A. Goddard III, J. Non-Cryst. Solids **253**, 133–142 (1999).
[66] R. L. Mozzi and B. E. Warren, J. Appl. Crystallogr. **2**, 164 (1969).
[67] J. R. G. Da Silva, D. G. Pinatti, C. E. Anderson, and M. L. Rudee, Philos. Mag.: J. Theor. Exp. Appl. Phys. **31**, 713 (1975).
[68] A. C. Wright, J. Non-Cryst. Solids **179**, 84 (1994), part of Special Issue: Proceedings of the First PAC RIM Meeting on Glass and Optical Materials.
[69] M. G. Tucker, D. A. Keen, M. T. Dove, and K. Trachenko, J. Phys.: Condens. Matter **17**, S67 (2005).